基于特征点测量的径向摩擦焊接温度场分布

张　磊[1]，　周　军[1]，　张春波[1]，　赵玉珊[1]，　秦国梁[2]
（1. 机械科学研究院 哈尔滨焊接研究所，哈尔滨　150080；2. 山东大学 现代焊接技术研究所，济南　250061）

张　磊

摘　要：介绍了半自然热电偶法测温原理，并对所选用的半自然热电偶进行了标定，线性度良好. 采用自主研发的径向摩擦焊机进行径向摩擦焊接工艺试验. 以摩擦焊接过程特点为依据，选择恰当的测温仪和热电偶. 采用半自然热电偶对径向摩擦焊接过程中摩擦界面中心点温度进行了全过程测量；采用 K 型热电偶对管体侧距界面中线点纵向距离为 1，2，3，6 mm 的位置进行了温度测量. 摩擦界面升温迅速，存在明显的温度恒定即稳定摩擦阶段. 随着距摩擦界面纵向距离的增加，升温速率逐渐降低，升温时间逐渐增长. 焊接过程结束后，温度逐渐趋于均匀化.

关键词：径向摩擦焊；　温度场；　温度测量
中图分类号：TG40　　**文献标识码**：A　　**文章编号**：0253－360X(2013)12－0071－04

0　序　　言

径向摩擦焊技术在海底管道连接及炮弹弹带连接领域具有不可替代的工艺优势[1,2]. 工艺适应性广、可靠性高、优质高效、绿色环保是其突出特点[3]. 国外从 20 世纪 70 年代开始，开展了基于海底管道连接的径向摩擦焊技术研究[4,5]. 代表研究机构为英国焊接研究所(TWI). 美国于 20 世纪 90 年代将该技术成功应用于弹带连接的实际生产中，代表研究公司为 MTI[1,6]. 国内关于径向摩擦焊的研究基本处于工艺探索和径向摩擦焊机优化阶段，对径向摩擦焊接机理的研究及物理量场的分析鲜有报道. 哈尔滨焊接研究所开展了《径向摩擦焊接过程中热力耦合的数值分析》研究工作[7,8]. 兵器工业集团第 59 研究所开展了《径向摩擦焊工艺研究》[9]工作.

摩擦焊属于固相连接技术，温度分布对焊接质量有着重要影响. 分析径向摩擦焊接头温度分布对研究径向摩擦焊接机理、提高焊接质量、优化工艺参数具有重要意义[9]. 目前，国内关于径向摩擦焊接头特征点温度的测量工作一直处于空白，对接头温度场的分析一直基于轴向摩擦焊积累的经验. 径向摩擦焊因其具有更复杂的压力加载方式以及工件变形过程，仅通过经验是不能客观分析其温度场分布的. 这也成为限制径向摩擦焊接机理研究及建立精确数值模拟模型的瓶颈.

文中对径向摩擦焊接头特征点温度进行了实际测量；对所选用的半自然热电偶进行了标定；采用半自然热电偶对径向摩擦焊接摩擦界面中心点的温度进行了全过程测量；采用 K 型热电偶对管体侧距界面中心点不同纵向距离的位置进行了温度测量. 通过分析特征点的温度变化规律，研究径向摩擦焊接头的温度场分布.

1　半自然热电偶测温原理及标定

图 1 为半自然热电偶测温法原理示意图. 该方法是标准热电偶法与自然热电偶法两者的结合. 选一根标准热电偶丝和径向环组成热电偶的两极，在摩擦界面上利用高温塑性金属层形成自然热接点，

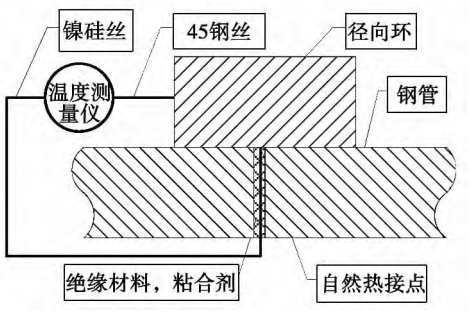

图 1　半自然热电偶测温法原理示意图
Fig. 1　Principle of semi natural thermocouple

收稿日期：2013－07－19
基金项目：国家自然科学基金资助项目(51075174)

根据该热接点所产生的热电势变化来测量摩擦界面温度. 很显然,这种方法的本质仍是一种热电势测温法,有关热电偶测温的基本理论、方法、设备均适用于该方法[10].

该方法一方面保持了自然热电偶法测量位置明确、动态响应快的长处,保证测点时刻位于摩擦界面上; 另一方面,吸取了标准热电偶测量点小的优点,使得能够测量界面上不同特征点的温度变化过程. 同时,由于标准偶丝的广泛选择性,克服了自然热电偶只适用于少数异种材料界面温度测量的缺点. 这种方法,对工件的材料几乎没有特殊要求. 适用于同种材料及异种材料的摩擦界面温度测量[10].

热电偶法是利用温度与热电势关系进行温度测量的测温手段. 所以要使用半自然热电偶,就必须标定其热电势与温度之间的对应关系. 文中标定了所选用的半自然热电偶基于 K 型分度表下的测量值与真实温度之间的对应关系.

由于径向环的材料是 45 钢,所以电极中自然热电偶一极的材质为 45 钢. 综合考虑价格、测量范围以及与 45 钢间的电特性曲线关系,标准热电偶一极选用 K 型热电偶中的镍硅丝. 其中 45 钢丝作为正极,镍硅丝作为负极.

文中选用 gleeble1500 热模拟试验机作为热源的提供仪器. 将标定的过程分成两个阶段,从室温到 800 ℃,每 100 ℃标定一次; 从 800 ~ 1 200 ℃,每 50 ℃标定一次. 用一级精度 K 型热电偶对热源温度进行采集监控.

热源的加载方式为: 15 s 升到设定温度,保温 10 s. 标定过程中对 K 型热电偶和半自然热电偶同时进行温度采集. 图 2 为标定结果. 其中标准热电偶测量值反映了温度加载过程的真实变化情况. 半自然热电偶的测量结果为基于 K 型分度表下的测量值.

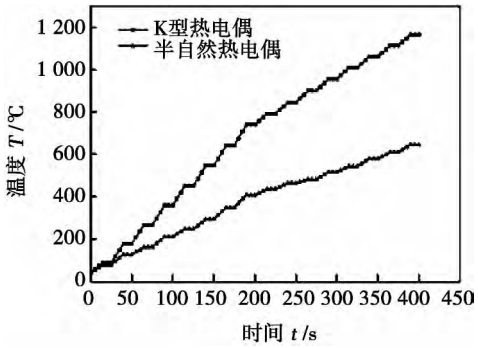

图 2 标定结果

Fig. 2 Calibration results

对图 2 中每一温度平台的测量值取平均值,将结果进行拟合,如图 3 所示. 将半自然热电偶测量值记为 X,K 型热电偶测量值记为 Y. 对数据进行拟合后得出的真实温度 Y 与半自然热电偶测量值 X 之间的线性函数关系为

$$Y = 1.899X - 37.2 \quad (1)$$

通过该函数关系即可将半自然热电偶的测量值与真实温度进行转换.

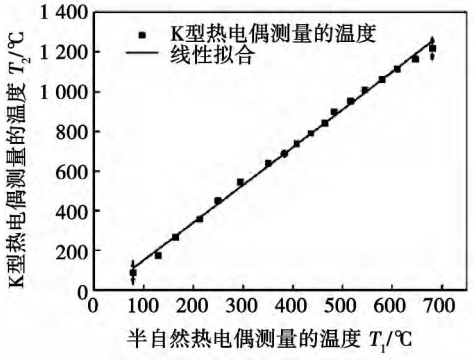

图 3 拟合结果

Fig. 3 Fitting result

2 试验方法

2.1 径向摩擦焊接试验

径向摩擦焊是摩擦焊接方法的一种,是依靠径向环与被焊工件(一般为管材或棒材) 之间摩擦运动产生的热量来实现材料可靠连接的一种热压焊方法. 图 4 为径向摩擦焊接过程示意图.

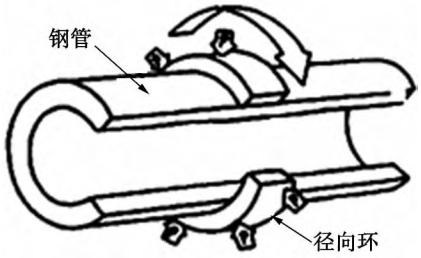

图 4 径向摩擦焊接过程示意图

Fig. 4 Diagram of radial friction welding

焊接时钢管固定不动,径向环在径向加载力及扭矩的作用下,内表面与钢管外表面相对高速摩擦,摩擦面上产生的热量把焊接区域的材料加热到适于锻造的温度,在径向力与扭矩作用下,将径向环与钢管牢固地焊接在一起.

试验设备为哈尔滨焊接研究所研发制造的 HSMZ-130 惯性轴径向多功能摩擦焊机,该设备可实现轴向焊接与径向焊接,如图 5 所示.

图 5　径向摩擦焊机

Fig. 5　Radial friction welding machine

试验材料为 45 钢,工件几何尺寸见表 1,摩擦焊接工艺参数见表 2,焊前试件见图 6.

表 1　工件几何尺寸

Table 1　Geometric dimensioning

工件	外径 d/mm	壁厚 t/mm	长度 l/mm
钢管	73	8	700
径向环	94	10	20

表 2　径向摩擦焊接工艺参数

Table 2　Geometric dimensioning

一级油压 p_1/MPa	二级油压 p_2/MPa	主轴旋转频率 n/(r·min^{-1})	转动惯量 J/(kg·m^{-2})
4	4.4	520	388

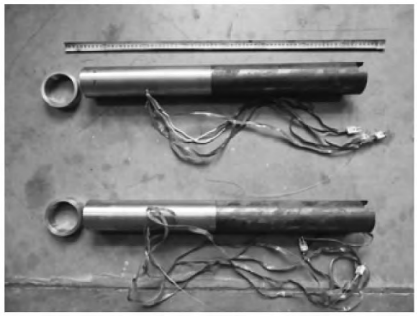

图 6　焊前试样准备

Fig. 6　Samples before welding

从表 1 可以看出,径向环的内径比钢管的外径大 1 mm. 焊接开始后,径向环在径向力的作用下向内收缩,当径向环的内径与钢管外径相等时,摩擦过程正式开始.

2.2　温度测量试验

摩擦焊接过程中,工件的摩擦界面是一个动态平面,摩擦界面附近塑性金属不断被挤出形成飞边. 整个过程中,摩擦界面附近金属发生着强烈的塑性变形和塑性流动,因此,要在焊接过程中实时测量摩擦面上的温度是相当困难的,标准热电偶法、红外测温法及红外成像法均不能实现摩擦界面温度的全过程测量.

文中选用半自然热电偶对摩擦界面中心点的温度进行全过程测量. 对于非摩擦界面处,选用 K 型热电偶,将其埋放在钢管侧距离摩擦界面中心点纵向距离为 1,2,3,6 mm 的位置进行温度测量. 由于径向摩擦焊接时间非常短,文中焊接时间为 2.9 s. 在焊接时间内,摩擦界面的温度经历了从室温 ~ 1 180 ℃,再迅速降温的过程. 因此需要选用高采样频率测温仪,及高响应速率热电偶丝才能将摩擦焊接过程的温度变化规律准确完整地采集出来. 热电偶的响应速率与偶丝的直径有关,直径越小,响应速率越高. 通过理论计算与实践验证,采样频率定为 20 Hz,偶丝直径选用 0.2 mm 较为合理. 由于焊接过程最高温度在 1 200 ℃以下,并且焊接时间非常短,因此标准偶丝选用 K 型热电偶. 测温仪如图 7 所示.

图 7　测温仪

Fig. 7　Thermodetector used in experiment

3　测量结果与分析

焊后试件如图 8 所示,测量结果见图 9. 从图 9 中可以看出,径向摩擦焊接过程中界面中心点的温度变化历程分为三个阶段: 初始摩擦阶段、稳定摩擦阶段和焊后冷却阶段. 由于焊接过程时间短,焊接阶段的界面温度主要取决于产热功率. 当径向环在径向力的作用下与钢管接触并开始摩擦时,界面温度开始急剧升高. 一方面,由于焊接压力高,界面温度低,故摩擦切应力大,对应摩擦扭矩急剧增大; 另一方面,此时主轴旋转频率高,所以此阶段加热速度最快. 初始摩擦阶段对应图 9 中 0 ~ 1.3 s. 最初的 0.4 s 内,径向环与钢管并未建立完全的接触,摩擦作用并不明显. 所以旋转频率只是略微下降,各采集点的温度略有升高. 从 0.4 s 开始,旋转频率迅速下降,同时界面的温度开始陡升.

稳定摩擦阶段,摩擦界面金属发生剧烈塑性变形. 摩擦扭矩由前峰值扭矩逐渐下降,主轴旋转频率不断降低,故摩擦产热功率降低. 该阶段对应图 9 中 1.3 ~ 2.6 s 时刻. 1.3 s 时刻后,界面升温速率开

图 8 焊后试样

Fig. 8 Joint of radial friction welding

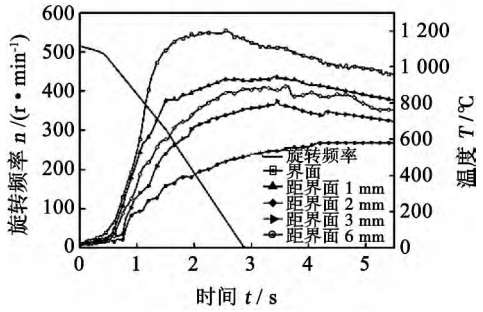

图 9 测量结果

Fig. 9 Temperature measurements

始变缓,1.7 ~ 2.9 s 时刻出现了一段温差小于 30° 的平稳台阶. 在此阶段,产热(摩擦生热、塑性变形产热)与散热(材料流动带走热量、热传导带走热量)达到动态平衡. 因此界面温度近乎恒定.

距界面 1,2,3 mm 位置处的温度与界面温度相比,变化较为平缓,升温速率依次降低,这是由于此处温度升高主要来源于热传导,所以越靠近界面的位置升温速度就越快. 并且越靠近界面的位置越早出现升温速率转变点,与界面的升温变化趋势越接近. 这是由于热量传递具有一定的滞后性,越接近界面的位置,受界面温度变化的影响越明显. 而越远离界面的位置受界面温度变化的影响越弱.

距界面 6 mm 位置处,温度变化更为平缓. 并且记录的时间内并未出现焊后降温阶段. 各点温度在焊后逐渐趋于均匀化.

4 结 论

(1) 通过标定试验得出所选用的半自然热电偶基于 K 型分度表测量值与真实值之间的函数关系,线性度良好.

(2) 采用半自然热电偶法对摩擦界面中心点温度进行测量,稳定摩擦阶段温度在 1 180 ℃以下.

(3) 采用标准热电偶法对管体侧距摩擦界面中心点不同纵向距离位置进行测量. 随着距摩擦界面纵向距离的增加,升温速率逐渐变缓,温度下降的起始时刻逐渐滞后.

参考文献:

[1] Xu Xiaoling, Wu Wei, Xu Yuanze, *et al*. The Research of radial friction welding [J]. Welding in the World, 2005, 49(1): 31 – 33.

[2] Kwietniewski C, Dos Santos J F, Da Silva A, *et al*. Effect of plastic deformation on the toughness behaviour of radial friction welds in Ti-6Al-4V-0.1 Ru titanium alloy [J]. Materials Science and Engineering: A, 2006, 417(1/2): 49 – 55.

[3] Maalekian M. Friction welding-critical assessment of literature [J]. Science & Technology of Welding & Joining, 2007, 12(8): 708 – 729.

[4] Nicholas E D, Lilly R H. Radial friction welding [J]. Recent Development in Pipeline Welding, 1979: 50 – 56.

[5] Singh J, Gill S S. Fuzzy modelling for burst pressure strength in radial friction welding of GI pipes [J]. International Journal of Modelling, Identification and Control, 2009, 7(3): 305 – 312.

[6] Wu W, Zhu L Y, Wu G F, *et al*. Study on performance of inertia radial friction welding of copper-alloy to 35CrMnSi steel [J]. Advanced Materials Research, 2011, 291: 968 – 974.

[7] 张 磊. 钢管径向摩擦焊温度场数值模拟 [D]. 北京: 机械科学研究总院, 2013.

[8] 张 磊, 秦国梁, 张春波, 等. 钢管径向摩擦焊温度场数值模拟 [J]. 焊接学报, 2013, 34(11): 32 – 36.
Zhang Lei, Qin Guoliang, Zhang Chunbo, *et al*. Numerical simulation on temperature field of radial friction [J]. Transcactions of the China Welding Institution, 2013, 34(11): 32 – 36.

[9] 张 磊, 赵玉珊, 张春波, 等. 摩擦焊焊接温度场测量研究现状 [J]. 焊接, 2012(10): 30 – 34.
Zhang Lei, Zhao Yushan, Zhang Chunbo, *et al*. Research progress of friction welding temperature field measurement [J]. Welding & Joing, 2012(10): 30 – 34.

[10] 杜随更, 段立宇, 吴诗惇, 等. 半自然热电偶测温法——一种测量摩擦界面温度及其分布的新方法 [J]. 焊接, 1996(7): 5 – 9.
Du Suigeng, Duan Liyu, Wu Shidun, *et al*. Temperature measurement with semi-thermal couple [J]. Welding & Joing, 1996(7): 5 – 9.

作者简介: 张 磊,男,1986 年出生,硕士. 主要从事摩擦焊及堆焊方面的科研工作. 发表论文 4 篇. Email: leibanzhanglei@163.com

通讯作者: 周 军,男,研究员. 硕士研究生导师. Email: mch_zhoujun@126.com

niversity, Chengdu 610500, China; 3. State Key Laboratory of Oil and Gas Reservoir Geology and Exploitation, Southwest Petroleum University, Chengdu 610500, China). pp 55 - 58

Abstract: The relationship between fatigue crack growth and self-emission magnetic signal for 20CrMo steel weld seam at the square wave load was studied by tension-tension fatigue experiment and metal magnetic memory test method. The characteristics of fatigue fracture were studied by SEM. The results show that with the increase of fatigue cycles, the self-emission magnetic signal of the weld seam increased, the fatigue crack growth rate firstly increases and then decreases before the crack reaches the weld. When the crack across the weld seam, with the increase of fatigue cycles, the self-emission magnetic signal of the weld seam begins to decrease, but the fatigue crack growth rate incrases rapidly. In different zones of the welded joint, the fatigue crack growth rates are different, the expansion rate for the heat-affected zone is faster , while in other regions the expansion rate is relatively slower. The fracture scanning analysis reveals that cleavage fatigue fracture occurs under the condition of square wave loads.

Key words: square wave loads; 20CrMo steel welding seams; metal magnetic memory; fatigue crack

Pulsed current parameters based control of aluminum alloy pulsed MIG welding process ZHANG Gang[1], HUANG Jiankang[1], SHI Yu[1], FAN Ding[1], LU Lihui[2], FAN Jiawei[3] (1. State Key Laboratory of Gansu Advanced Non-ferrous Metal Materials, Lanzhou University of Technology, Lanzhou 730050, China; 2. School of Electric Information and Automation, Qufu Normal University, Rizhao 276826, China; 3. Gansu Tobacco Industry Co., Ltd., Lanzhou 730050, China). pp 59 - 62

Abstract: Weld appearance and stability of pulsed MIG welding process of aluminum alloy mainly depend on the stability of arc length. In order to obtain the stable welding process and high quality weld bead, the influence of pulsed current parameters on the stability of arc length was studied by welding experiments. The dynamical mathematical model between pulsed current parameters and arc length was established. Meanwhile, the dynamical response of arc length was simulated by varying duty-ratio and frequency of pulsed current based on Matlab/Simulink software. At last, the welding experiments were carried out when the duty-ratio and frequency of pulsed current were changed, respectively. The result shows that the established model can reflect the variation of pulsed MIG welding process very well, and the stable welding process can be obtained through changing duty-ratio and frequency of pulsed current, and the sound weld shape was obtained.

Key words: pulsed MIG welding of aluminum alloy; modeling and simulation; pulsed current parameters; process control.

Fundamental research of welding plastic strain evolution process: Characteristics and law of evolution process of welding plastic strain in mild steel, stainless steel and titanium alloy thin plate WANG Peng[1], XIE Pu[1], ZHAO Haiyan[1], GUAN Qiao[2] (1. Department of Mechanical Engineering, Tsinghua University, Beijing 100084, China; 2. Beijing Aeronautical Manufacturing Technology Research Institute, Beijing 100024, China). pp 63 - 66

Abstract: The evolution processes of arc welding plastic strain in mild steel, stainless steel and titanium alloy thin plate were analyzed by using numerical simulation method, respectively. Comparing with the measurement results, the calculation results demonstrate that both of longitudinal and transverse plastic strains in the weld and near weld zone during the welding process are compress plastic strain. The tensile unloading generated in the cooling stage cannot compensate the pre-existing compress plastic strain, which makes the residual plastic strain in the weld and near weld zone remain in compressive state. The width of compress plastic strain area is obviously wider than that of "materials´mechanics melting zone". Welding speed has a significant effect on residual plastic strain and stress in titanium alloy plate.

Key words: mild steel; stainless steel; titanium alloy; welded plastic strain; finite element analysis

Weld appearance of 2219-T87 high strength aluminum alloy at different pulse frequency LI Yulong, CONG Baoqiang, QI Bojin, YANG Mingxuan (School of Mechanical Engineering and Automation, Beihang University, Beijing 100191, China). pp 67 - 70

Abstract: Based on hybrid ultrahigh frequency pulse variable polarity gas tungsten arc welding process of 2219-T87 high strength aluminum alloy, the effect of pulse frequency on weld appearance was analyzed. Experimental results show that the pulse frequency has a great impact on arc characteristics and the molten pool flow behavior, which makes significant changes in the weld width, depth and penetration. When the pulse frequency f_H is less than 60 kHz, the weld width and depth increase with the increase of pulse frequency. The weld penetration is hardly changed with $f_H < 35$ kHz, while it is considerably improved by at least 34% compared with the conventional variable polarity GTAW process when $f_H > 35$ kHz. When the pulse frequency reached up to 60 kHz, the weld penetration significantly increases by 60% compared with the conventional variable polarity GTAW process. When the pulse frequency $f_H > 65$ kHz, the weld width, depth and penetration presented show the downward trend.

Key words: high strength aluminum alloy; pulse current; weld appearance; gas tungsten arc welding

Radial friction welding temperature field based on temperature measurement of feature points ZHANG Lei[1], ZHOU Jun[1], ZHANG Chunbo[1], ZHAO Yushan[1], QIN Guoliang[2] (1. Harbin Welding Institute, China Academy of Machinery Science and Technology, Harbin 150080, China; 2. Institute of Materials Joining, Shandong University, Jinan 250061, China). pp 71 - 74

Abstract: The principle of semi-natural thermocouple to measure the temperature was introduced and the semi-natural thermocouple was calibrated with good linearity. Radial friction welding process was carried out with the relf-design radial friction welding machine. Based on the friction welding process characteristics, the appropriate thermometer and thermocouple were selected. The temperature on the friction interface was tested with

the semi-natural thermocouple. The points on different distance from the interface were measured with K type thermocouple. The temperature on the friction interface rises quickly and there is an obvious stage with constant temperature. With the increase of distance from friction interface, the rising rate of the temperature decrease gradually. After the welding process, the temperature gradually tends to be homogenous.

Key words: radial friction welding; temperature field; temperature measurement

Geometric size effect on interfacial elements diffusion of Cu/SAC305/Cu micro-structure LUO Liangliang, SUN Fenglian, ZHU Yan (College of Materials Science and Engineering, Harbin University of Science and Technology, Harbin 150040, China). pp 75 - 78

Abstract: The relation between solder thickness and the growth behavior of IMC during HTS (high-temperature storage) aging was investigated with Cu/SAC305/Cu sandwich structures at different solder thicknesses (15 ~ 50 μm). The results indicated that the solid state diffusion of interfacial elements is greatly dependent upon solder thickness during HTS aging. The thinner the solder layer is, the faster the Cu_3Sn layer grows, which leads to a thickness ratio decrease of Cu_6Sn_5/Cu_3Sn after HTS aging at 160 ℃. The growth rate of IMC layer (Cu_6Sn_5 layer + Cu_3Sn layer) also decreases with the decrease of solder thickness during HTS aging. The diffusion coefficient is in relation with the size of solder layer. Further data correlating indicates that the alternation regularity between diffusion coefficient and solder thickness is approximately accordance with parabolic correlation.

Key words: high-temperature storage aging; intermetallic compounds; diffusion coefficient; geometrical size effect

Numerical research on weld bead geometry and residual stresses with different heat source models in laser welding of TC4 titanium alloy LI Xingxia[1], WANG Hongyu[2], ZHANG Jianxun[2] (1. Department of Materials Engineering, Henan Mechanical and Electrical Engineering College, Xinxiang 453002, China; 2. State Key Laboratory for Mechanical Behavior of Materials, Xi´an Jiaotong University, Xi´an 710049, China). pp 79 - 82

Abstract: According to the features of laser deep penetration welding, three heat models of uniform heat source, double ellipsoidal heat source and the combined heat source were used to study numerically the weld bead geometry and residual stresses in CO_2 laser welding of TC4 titanium alloy. The results show that the heat source model in calculation should be selected according to the energy input. Then an approach to select the heat source model was proposed that the uniform heat source should be used under the condition of the greater energy input, the double ellipsodial heat source is suitable for medium energy input and the combined heat source fits for smaller energy input. Both the double ellipsodial heat source and the combined heat source can indicate the decrease of heat input with depth, and the estimated weld bead geometry as circular cone shape or nail shape. The residual stresses on top and back sides are similar when the uniform heat source is used, but the larger residual stress exists on the top surface than that on back surface when the double ellipsodial and combined heat sources are used.

Key words: laser welding; heat source model; titanium alloy

Analysis of arc adjustment mechanism to pulsed MIG welding based on PFM adjustment ZHANG Xiaoli[1,2], LIN Fang[3], LI Yuzhen[2], XUE Jiaxiang[2] (1. College of Mechanical and Electrical Engineering, Jiangxi University of Science & Technology, Ganzhou 341000, China; 2. School of Mechanical and Automotive Engineering, South China University of Technology, Guangzhou 510640, China; 3. Department of Electromechanical, Jiangmen Polytechnic College, Jiangmen 529000, China). pp 83 - 87

Abstract: Aimed at the problems of arc length control in pulsed MIG welding power supply, the research of arc self-regulating mechanism and arc adjusting mechanism under the control of the pulse frequency modulation (PFM) was developed. The mathematical model of arc length was established. The principle of PFM arc adjustment system was introduced and the PFM current regulation model was given. The PFM arc control mechanism and the problems existing in the arc control were analyzed for non-resistance wire and resistance wire. A more stable welding effect can be obtained for PFM current regulation of non-resistance wire from theoretical derivation. For the resistance wire, the stable welding effect can be obtained when CTWD is fixed and satisfactory welding results cannot be obtained while CTWD changing. Finally the step tests of PFM arc adjustment were carried out by using non-resistance wire and resistance wire, respectively. The theory above is verified by test results.

Key words: PFM adjustment; pulsed MIG welding; arc; resistance wire; non-resistance wire

Numerical simulation of ultrasonic impact treatment on 6061 aluminum alloy welding residual stress CHEN Jian, LÜ Lin, FANG Kai (Jiangsu Provincial Lab of Advanced Welding Technology, Jiangsu University of Science and Technology, Zhenjiang 212003, China). pp 88 - 92

Abstract: The ultrasonic impact treatment on the thin 6061 aluminum alloy plate without and with welding residual stress was analyzed by means of the finite element software ANSYS. The simulated result was compared with the tested one. In the case of the existence of no welding residual stress, the result shows that the surface stresses are compressive at the impact center, and tensile around the center after treatment. Along the depth of the sample, compressive stresses turn into tensile ones. The whole stress state increases gradually with the treatment. In the case of the existence of welding residual stress, with the increase of the displacement load, stresses at the impact zone decrease greatly and the highest stress locates the area away from the weld. The simulated result of the stress change accords well with the tested one.

Key words: ultrasonic impact treatment; welding residual stress; numerical simulation

Welding groove model and accuracy of processing technology of square tube REN Qingchuan, XU Lei, HUANG Shiyou, YE Zhenzhen (School of Manufacturing Science & Engineer-